Applied Catalysis B: Environmental 232 (2018) 275–287

Contents lists available at ScienceDirect

Applied Catalysis B: Environmental

journal homepage: www.elsevier.com/locate/apcatb

Ag-Cu based catalysts for the selective ammonia oxidation into nitrogen and water vapour

Magdalena Jabłońska[a,b,*], Andrew M. Beale[c,d], Marek Nocuń[e], Regina Palkovits[a,b,*]

[a] Institut für Technische und Makromolekulare Chemie, Chair of Heterogeneous Catalysis and Chemical Technology, RWTH Aachen University, Worringerweg 2, 52074, Aachen, Germany
[b] Center for Automotive Catalytic Systems Aachen-ACA, RWTH Aachen University, Schinkelstr. 8, 52062, Aachen, Germany
[c] Department of Chemistry, University College London, 20 Gordon Street, London, WC1H 0AJ, UK
[d] Research Complex at Harwell, Rutherford Appleton Laboratories, Harwell Science and Innovation Campus, Harwell, Didcot, Oxon, OX11 0FA, UK
[e] Faculty of Material Science and Ceramics, AGH University of Science and Technology, Mickiewicza 30, 30-059, Kraków, Poland

ARTICLE INFO

Keywords:
Alumina
Silver oxide species
Copper oxide species
Selective ammonia oxidation
Reaction mechanism

ABSTRACT

XRD, BET, H_2-TPR, UV–vis-DRS, XPS and XAFS were used to characterize a series of Ag and/or Cu – Ag (1–5%), Cu (10–15%) or Ag-Cu (1–1, 1–10, 1.5–10, 5–5% of metal) – supported on γ-Al_2O_3. Correlation between physicochemical properties, catalytic activity and selectivity in NH_3-SCO were thoroughly investigated. Silver species mainly in the form of Ag_2O on the Ag/Al_2O_3 catalysts led to enhanced activity together with drop in N_2 selectivity with increasing silver loading up to 5%. A mixture of CuO and $CuAl_2O_4$ formed on the Cu/Al_2O_3 catalysts. Easily reducible highly dispersed CuO_x promoted the activity of the catalysts, while bulk CuO_x and $CuAl_2O_4$ decreased N_2 selectivity up to 500 °C. The activity of all Cu-containing materials was inferior to Ag-containing ones. Thus, the gap between the high conversion temperature over Cu/Al_2O_3 and low N_2 selectivity over Ag/Al_2O_3 was bridged by applying the $Ag\text{-}Cu/Al_2O_3$ catalysts, with the optimum loading of 1.5 and 10 wt.% for silver and copper, respectively. NH_3-TPD, NH_3-TPSR and *in situ* FTIR were used to determine the *in situ* selective catalytic reduction (i-SCR) mechanism over 1.5% Ag/Al_2O_3, 10% Cu/Al_2O_3 and 1.5% Ag-10% Cu/Al_2O_3 respectively. The i-SCR mechanism involved the partial oxidation of NH_3 into NO_x species, along with adsorbed NO_x species interacting with adsorbed ammonia (NH_x species) and being reduced to reaction products.

1. Introduction

Ag-based catalysts, including silver supported on γ-Al_2O_3, serve as one of the most active and N_2 selective materials for the selective catalytic ammonia oxidation into nitrogen and water vapour (NH_3-SCO) below 300 °C [*e.g.* [1–3]. Qu et al. [1] studied silver supported on γ-Al_2O_3, TiO_2, SiO_2 or NaY, and found that catalytic activity and selectivity depended strongly on the size and distribution of silver species. Highly dispersed Ag^0 particles with a size of 5 nm were obtained on H_2-pretreated 10% Ag/Al_2O_3 and reported as the most active and N_2 selective in NH_3-SCO below 140 °C (full conversion and 89% of N_2 selectivity at 180 °C). Ag^+ was the main active species responsible for the high catalytic performance above 140 °C. A significantly lower selectivity to N_2 (around 60–80% at 180 °C) over a similar catalyst – 10% Ag/Al_2O_3, was reported by Zhang et al. [2] or Gang et al. [4]. These discrepancies appeared possibly due to different preparation procedures of the catalysts. Nevertheless, above 300 °C, selectivity to N_2 decreased significantly over Ag/Al_2O_3 due to formation of NO over Ag_2O [5]. On the other hand, copper-based catalysts possess high intrinsic activity in the oxidation of ammonia with an excellent selectivity to N_2 at high temperatures. The copper-based materials containing about 10% of Cu were recognized as one of the most efficient catalysts in NH_3-SCO [6]. Thus, the proper mixing of silver with copper leads to highly active and selective bifunctional catalytic system, in which silver species catalyse ammonia oxidation to NO_x, while copper oxide species perform the reduction of NO_x to nitrogen [5,7]. Yang et al. [5] studied $Ag\text{-}Cu/Al_2O_3$ with 5–5 or 10–10% of metal and indicated the material with the first composition as highly efficient catalysts with complete conversion temperature at 325 °C and 95% N_2 selectivity. Unfortunately, the authors did not present results of catalytic tests above 350 °C. Gang et al. [8] investigated 7.5% Ag-2.5% Cu/Al_2O_3 and found full conversion of ammonia at 200–300 °C with 95% N_2 selectivity. Both activity and selectivity to N_2 significantly increased compared to Ag/Al_2O_3. Nevertheless, above 300 °C significant amounts of NO and N_2O

* Corresponding authors at: Institut für Technische und Makromolekulare Chemie, Chair of Heterogeneous Catalysis and Chemical Technology, RWTH Aachen University, Worringerweg 2, 52074 Aachen, Germany.
E-mail addresses: Jablonska@itmc.rwth-aachen.de (M. Jabłońska), Palkovits@itmc.rwth-aachen.de (R. Palkovits).

https://doi.org/10.1016/j.apcatb.2018.03.029
Received 18 September 2017; Received in revised form 2 March 2018; Accepted 9 March 2018
Available online 11 March 2018
0926-3373/

appeared over Ag-Cu/Al_2O_3. Interestingly, a mechanical mixture of 10% Ag/Al_2O_3 and 10% Cu/Al_2O_3 showed similar catalytic performance to a silver-based catalyst alone. Thus, the intimate contact between the silver species and copper species – active species dedicated for ammonia oxidation to NO_x and reduction of NO_x to nitrogen, respectively – led to shorter diffusion length and consequently improved catalytic activity and N_2 selectivity. The authors applied XPS measurements over 5–5, 7.5–2.5% Ag-Cu/Al_2O_3, which revealed the same oxidation state as for single 10% Ag/Al_2O_3 or 10% Cu/Al_2O_3. Additionally, LEIS analysis over 10–2.5, 2.5–7.5, 5–5, 9–1% Ag-Cu/Al_2O_3 excluded formation of any Ag-Cu phases. Besides studies of Gang et al. [8], up to now and to the best of our knowledge no other studies devoted to the correlations between the state of silver and/or copper oxide species in Ag-Cu/Al_2O_3 on the catalytic activity and N_2 selectivity in the ammonia oxidation have been reported. The structure-activity relationship of the bimetallic Ag-Cu/Al_2O_3 catalysts with lower silver loading (1–5%) remains ambiguous. Thus, we focused on characterization of bimetallic Ag-Cu/Al_2O_3 in comparison to monometallic Ag/Al_2O_3 and Cu/Al_2O_3, and determination of the influence of metal loading on the physicochemical properties obtained and their catalytic activity and selectivity in the selective ammonia oxidation into nitrogen and water vapour. Preliminary results revealed that silver increased activity of the Ag-Cu catalysts in the low-temperature range but also significantly decreased selectivity to nitrogen. Accordingly, we focused on the determination of the optimal content of silver and copper, guaranteeing optimum activity together with N_2 selectivity. We investigated different amounts of Ag (1.0–5.0%), Cu (10–15%) or Ag-Cu (1–1, 1–10, 1.5–10, 5–5% of metal) on the γ-Al_2O_3 support. Secondly, we concentrated our attention on the interaction between silver and copper oxide species deposited on the surface of the Al_2O_3 support, thus, this approach enabled the comparison of the role of active components in NH_3-SCO between 50 and 350 °C.

2. Experimental part

2.1. Catalyst preparation

γ-Al_2O_3 (Merck) was doped with Ag and/or Cu by the incipient wetness impregnation using aqueous solutions of $Cu(NO_3)_2{\cdot}3H_2O$ (Sigma-Aldrich) and $AgNO_3$ (Sigma-Aldrich). In the bimetallic systems, after impregnation with aqueous solution of copper salt, the sample was first dried at 80 °C overnight followed by impregnation with aqueous solution of silver salt. All prepared samples were dried and subsequently calcined in static air at 600 °C for 12 h. For catalytic experiments, a sieve fraction of particles with size of 0.250–0.500 mm was used. The weight ratio of metals was measured with respect to the mass of γ-Al_2O_3.

2.2. Catalyst characterization

The X-ray diffraction (XRD) patterns of the samples were recorded in flat plate mode in Bragg-Brentano geometry using a D5000 Siemens diffractometer and a Cu Kα source (λ = 1.54056 Å, 45 kV, 40 mA).

The specific surface area (S_{BET}) of the samples was determined by low-temperature (−196 °C) N_2 sorption using Quantachrome Quadrasorb SI. Prior to nitrogen adsorption the samples were outgassed at 250 °C for 12 h using a Quantachrome Flovac degasser. The specific surface area (S_{BET}) was calculated using the Brunauer-Emmett-Teller (BET) multiple point method at partial pressures from p/p_0 range from 0.05 to 0.3. The total pore volume was determined at p/p_0 = 0.99.

The temperature-programmed reduction (H_2-TPR) experiments of samples (30 mg) were performed using a Quantachrome ChemBET Pulsar TPR/TPD instrument. H_2-TPR runs were carried out starting from room temperature to 1000 °C, with a linear heating rate of 10 °C min^{-1} and in a flow (25 ml min^{-1}) of 5 vol.% H_2 diluted in Ar. Water vapour was removed from effluent gas by the means of a cold trap placed in an ice-water bath. The H_2 consumption was detected and recorded by TCD detector.

The diffuse reflectance UV–vis (UV–vis-DR) spectra of the samples were recorded using a Perkin-Elmer Lambda 7 UV–vis spectrophotometer. The measurements were performed in the range of 200–900 nm with the resolution of 1 nm. The spectra were recorded under ambient conditions and the data transformed according to the Kubelka-Munk equation.

The X-ray photoelectron spectra (XPS) of selected samples were measured on a VSW spectrometer equipped with a hemispherical analyser. The photoelectron spectra were measured using a magnesium MgKα source (1253.6 eV). The base pressure in the analysis chamber during the measurements was 3×10^{-6} Pa and the spectra were calibrated on a main carbon C 1s peak at 284.6 eV. The composition and chemical surrounding of the sample surface were investigated based on the areas and binding energies of Ag 3d, Cu 2p, Al 2p, C 1s and O 1s photoelectron peaks. Mathematical analyses of the XPS spectra were carried out using the XPSpeak 4.1 computer software (RWM. Kwok, The Chinese University of Hong Kong).

The X-ray absorption spectra (XAS) of selected samples were performed at room temperature on station B18 at the ESRF at the Diamond Light Source national synchrotron facility. The station is equipped with a Si(111)/Si(311) double crystal monochromator, and ion chambers for measuring incident and transmitted beam intensities for recording X-ray absorption spectra. The measurements were carried out using a Si (111) monochromator at the Ag K-edge or Cu K-edge with the respective Ag or Cu monometallic foil (10 μm) used as an energy calibrant for the monochromator. Measurements were performed in quick scanning mode; the time taken for each scan was *ca.* 5 min (a step size of 0.5 eV and counting time of 1/6 s/point was used for collection of data around the edge). To improve the signal-to-noise ratio, multiple scans were taken. Samples were pressed into 13 mm pellets using an appropriate amount of cellulose as binder and submitted to ex-situ XAFS experiments. All data were subjected to background correction using Athena (*i.e.* IFFEFFIT software package for pre and post edge background subtraction and data normalization [9,10]). XAFS spectra were normalized from 30 to 150 eV above the edge energy, while the EXAFS were normalized from 150 eV to the last data point using the Autobk algorithm. Normalization was performed between μ(E) and μ0(E) *via* a line regression through the data in the region below the edge and subtracted from the data. A quadratic polynomial is then regressed to the data above the edge and extrapolated back to E0. The extrapolated value of the post edge polynomial at E0 is used as the normalisation constant. This threshold energy (E0) was determined using the maximum in the 1st derivative. A calibration curve derived from the references was used to determine oxidation states from the edge position obtained from the maximum in the first derivative of the measured XANES spectra of the selected samples. The normalized isolated EXAFS data were k^3-weighed and a least squares fitting analysis was performed over a *k*-range of 0.3–0.8 nm^{-1} (Ag) otherwise 0.3–1.1 nm^{-1} (Cu). The FT of the k^3-weighed data were phase corrected and fit (using single scattering paths) to the proposed theoretical model using the DL-EXCURV program. An amplitude reduction factor (S_o^2) value of 0.95 was used for all data sets. Errors in the determination of the parameters derived from the fitting of the EXAFS data were estimated to be 10% of the coordination number and Debye-Waller factor and ~0.002 nm for bond distance.

2.3. Catalytic tests

The catalytic experiments of selective ammonia oxidation (NH_3-SCO) were performed under atmospheric pressure in a fixed-bed flow microreactor (i.d., 6 mm; l., 320 mm). The reactant concentrations were continuously monitored using a QMS MKS Cirrus 2 detector directly connected to the reactor outlet using a heated capillary. Prior to the test the sample of catalyst (100 mg) was outgassed at 500 °C for 1 h in a flow

of pure argon (20 ml min^{-1}). The composition of the gas mixture at the reactor inlet consisted of 0.5 vol.% NH_3, 2.5 vol.% O_2 diluted in Ar. The individual flow rates were controlled by Bronkhorst mass flow controllers. The total flow rate of the reaction mixture was 40 ml min^{-1}, while the weight hourly space velocity (WHSV) was about 24,000 ml h^{-1} g^{-1}. The studies were performed in the temperature range of 100–500 °C with the linear heating rate of 5 °C min^{-1}. For selected sample additional catalytic tests: (i) polythermal in the presence of water vapour and (ii) isothermal NH_3-SCO were carried out with the following composition of the gas mixture of 0.5 vol.% NH_3, 2.5 vol.% O_2, ([H_2O] = 3.2 vol.%) diluted in Ar. The signal of the argon line served as the internal standard to compensate small fluctuations of the operating pressure. The sensitivity factors of the analysed lines were calibrated using commercial mixtures of the gases.

2.4. Temperature-programmed desorption (NH_3-TPD) and temperature-programmed surface reaction (NH_3-TPSR)

The NH_3-TPD and NH_3-TPSR were performed in a fixed-bed flow microreactor (i.d., 6 mm; l., 320 mm) equipped with a QMS MKS Cirrus 2 detector. Prior to the ammonia sorption the sample (100 mg) was outgassed in a flow of pure argon (20 ml min^{-1}) at 500 °C for 1 h. Subsequently, the microreactor was cooled down to 70 °C and the sample was saturated with 1 vol.% of NH_3 diluted in Ar (2 h, 20 ml min^{-1}). Afterwards, the sample was purged in a flow of Ar until a constant baseline level was reached (2 h, 20 ml min^{-1}). For desorption step the temperature of the microreactor was raised form 70 up to 500 °C with a linear heating rate of 5 °C min^{-1} in a flow of pure argon (NH_3-TPD) or in a flow of 5 vol.% of O_2 diluted in Ar (NH_3-TPSR). The total flow rate in both measurements was 20 ml min^{-1}.

2.5. Fourier transform infrared spectroscopy

The *in situ* DRIFT spectra were recorded with a Vertex 70-FTIR Bruker spectrometer equipped with a MCT detector. Prior to the FTIR study the sample was pretreated *in situ* at 400 °C in a flow of pure N_2 for 1 h and then cooled to 50 °C. The sample was saturated in a flow (5 ml min^{-1}) of gas mixture containing 1.0 vol.% of NH_3 diluted in Ar for about 0.5 h. Subsequently, the physisorbed molecules were removed in 15 min evacuation. Next, the sample contacted with NH_3 was heated in a flow of: (i) pure N_2 or (ii) 5.0 vol.% O_2 diluted in Ar up to 100–350 °C, kept at particular temperature for 10 min and cooled down to 50 °C, while the spectrum was collected. All spectra were recorded at a resolution of 4 cm^{-1} with 128 accumulated scans. The background spectrum was subtracted from the sample spectrum.

3. Results and discussion

The XRD analysis allowed the identifications of the crystalline phases present in the Ag-Cu-based materials. The characteristic XRD diffraction peaks corresponding to the reflections of γ-Al_2O_3 were located at about 20, 33, 38, 40, 46, 61 and 67° 2θ [11]. As shown in Fig. 1A, no changes in the structure of the oxide support appeared after impregnation with Ag below 5%. However, for the sample with 5% of silver, Ag_2O was emphasised by reflexes at 34 and 39° 2θ [12], besides the peaks assigned to the support. Fig. 1B presents the XRD diffraction pattern of Cu/Al_2O_3 with different copper loadings. Diffractions for CuO (2θ angle of 35, 38, 48, 53, 58, 62, 66 and 68° [13]) arose when the copper in the samples increased to 10–15%. Besides the reflections ascribed to CuO, a XRD reflex attributable to $CuAl_2O_4$ at 37° 2θ could not be excluded [14]. The reflections characteristic of Ag_2O, CuO and $CuAl_2O_4$ appeared also in Ag-Cu bimetallic systems, as depicted in Fig. 1C. The formation of bulk CuO and/or Ag_2O was related to agglomeration of transition metal oxide species, presumably due to saturation of the Al_2O_3 support.

BET analyses provided the evolution of specific surface areas (S_{BET}) and total pore volumes (V_p) of the Ag-Cu-based materials. As presented in Table 1, Al_2O_3 revealed a S_{BET} and total pore volume of about 135 m^2 g^{-1} and 0.2393 ml g^{-1}, respectively. The deposition of transition metal oxides within the pore system of the γ-Al_2O_3 support resulted in a decrease of S_{BET} and V_p, especially for metal loading higher than 5%. The total pore volume dropped with increasing amount of transition metals until 0.2097 ml g^{-1} and 0.1981 ml g^{-1} for 5% of Ag and 15% of Cu, respectively. Also, the Ag-Cu bimetallic systems showed S_{BET} and V_p lower compared to the Al_2O_3 support. As a result of differences between silver and copper oxides, the specific surface area and total pore volume varied appreciably in the bimetallic Ag-Cu materials.

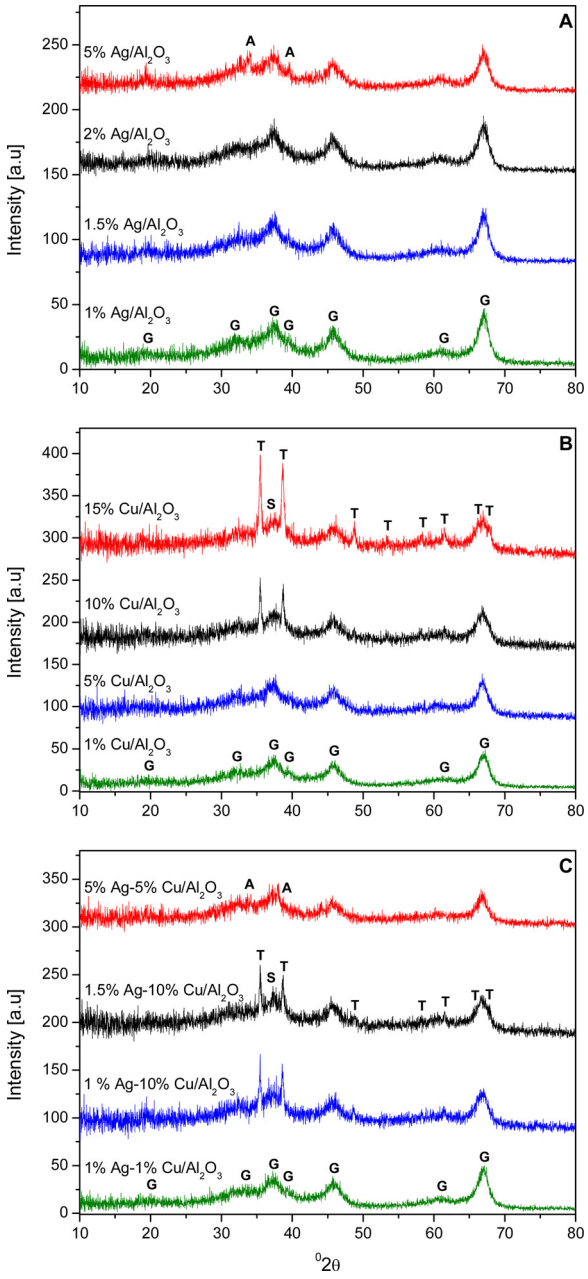

Fig. 1. XRD patterns of Ag/Al_2O_3 (A), Cu/Al_2O_3 (B), Ag-Cu/Al_2O_3 (C); G – γ-Al_2O_3, A – Ag_2O, T – CuO, S – $CuAl_2O_4$.

The H_2-TPR analysis provided insight into redox properties of silver and/or copper species in the Ag-Cu-based materials. Fig. 2A and C shows the H_2-TPR profiles of Ag-based catalysts. A low-temperature peak appeared in the H_2-TPR profiles of Ag-modified samples, indicating reduction of highly dispersed Ag_2O [15,16]. The maximum of the reduction shifted to higher temperatures (from 113 to 125 °C for 1

Table 1
Specific surface areas (S_{BET}) and total pore volumes (V_p) of the Ag/Al_2O_3, Cu/Al_2O_3, $Ag-Cu/Al_2O_3$.

Sample codes	S_{BET} [$m^2 g^{-1}$]	V_p [$ml\,g^{-1}$]
Al_2O_3	135	0.239
1% Ag/Al_2O_3	127	0.223
1.5% Ag/Al_2O_3	125	0.218
2% Ag/Al_2O_3	124	0.218
5% Ag/Al_2O_3	118	0.210
1% Cu/Al_2O_3	126	0.247
5% Cu/Al_2O_3	117	0.210
10% Cu/Al_2O_3	114	0.199
15% Cu/Al_2O_3	111	0.198
1% Ag-1% Cu/Al_2O_3	128	0.230
1% Ag-10% Cu/Al_2O_3	112	0.200
1.5% Ag-10% Cu/Al_2O_3	105	0.180
5% Ag-5% Cu/Al_2O_3	101	0.206

to 5% of Ag, respectively) with the increasing loading of silver, indicating partial aggregation of silver oxide species. Jabłońska et al. [17] showed two peaks (at 110 and 385 °C) in the H_2-TPR of analogues Ag/Al_2O_3 samples with 1% of silver loading. Thus, the sample contained highly dispersed, as well as Ag_2O clusters. These discrepancies appeared possibly due to different set-up arrangement as well as conditions of H_2-TPR measurements (total flow of 25 *versus* 6 ml min^{-1}). For the sample with 5% of Ag, an additional peak appeared at about 565 °C due to reduction of Ag_2O clusters [16]. As shown in Fig. 2B and C, H_2-TPR profiles changed also with different copper loading, suggesting formation of different copper oxide species. The reduction of Cu/Al_2O_3 with 1% of copper, consisted of three reduction peaks appearing at about 350, 615 and 775 °C, which is consistent with earlier results of Jabłońska et al. [18]. The first peak appeared due to the reduction of highly dispersed CuO_x. The peaks located at higher temperatures were related to the reduction of bulk CuO_x and defective spinel-type surface $CuAl_2O_4$, respectively. $CuAl_2O_4$ – with most Cu^{2+} ions in a distorted octahedral geometry – was formed between CuO and Al_2O_3 as a result of their interaction at 600 °C [19,20]. For higher copper loading (5%), the peak appeared due to the reduction of highly dispersed CuO_x on the Al_2O_3 surface. This peak spread into two peaks with increasing amount of copper. The H_2-TPR profiles for the samples with 10 and 15% of Cu showed low and high temperatures reduction peaks at about 261–273 °C and 303–315 °C, respectively. The peaks centered at 303–315 °C appeared due to reduction of bulk CuO_x and $CuAl_2O_4$ on the catalysts surface [20]. The peaks at 615 and 775 °C were not recorded for the samples with higher copper loading (5–15%) due to increasing particle size of copper oxide species exhibiting higher reducibility. As confirmed from XRD analysis, the intensity of CuO increased in line with the copper loading on the Al_2O_3 support. The reducing temperatures of the highly dispersed CuO_x for Cu/Al_2O_3 with 10% of copper appeared at lower temperatures than for materials with other copper loadings, indicating that a redox cycle would occur easier. H_2 uptake (calculated by equation: $Y = 1E-08X + 1E-07$, $R^2 = 0.9996$, and X, Y referred to the area of each reduction peak and the H_2 consumption, respectively) increased from 0.59, 1.02 up to 1.95 mmol g^{-1} for the samples with 5, 10 and 15% of copper loading, respectively. Quantification of H_2 consumption suffered from fluctuations of the baseline in H_2-TPR profiles of material with small amount of copper (1%) as well as Ag-(Cu)-containing materials.

The coexistence of silver and copper oxide species in the Ag-Cu bimetallic systems resulted in a shift of the H_2-TPR maximum peaks to lower temperatures. As shown in Fig. 2C, the H_2-TPR profile for a sample with 1% of both Ag and Cu consisted of a main broad peak centered at about 227 °C. An even more significant shift to lower temperatures appeared for sample with 5% of both metals, as presented in Fig. 2D. The materials with 1–1.5% of Ag and 10% of Cu showed similar H_2-TPR profiles; however, the sample with higher silver loading (1.5%

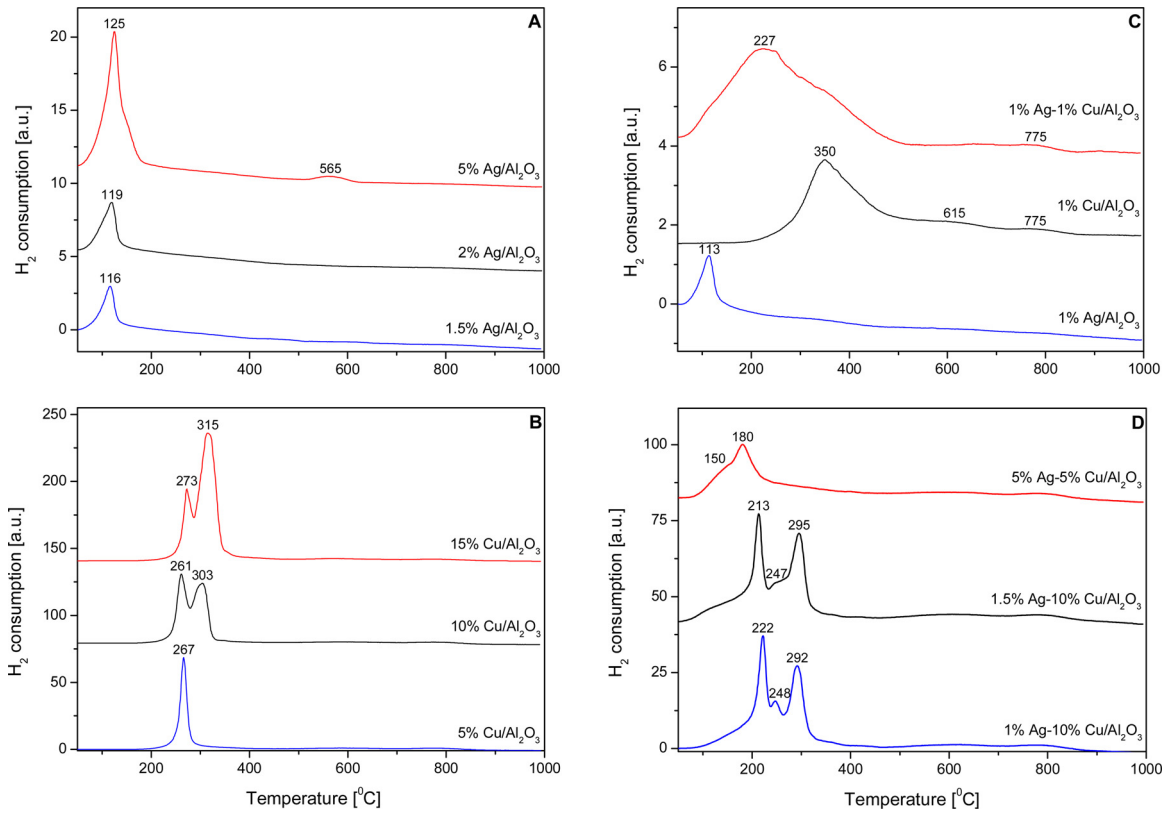

Fig. 2. H_2-TPR profiles of Ag/Al_2O_3 (A,C), Cu/Al_2O_3 (B,C), $Ag-Cu/Al_2O_3$ (C,D); experimental conditions: mass of the catalysts = 30 mg; [H_2] = 5.0 vol.%, Ar balance, flow rate = 25 ml min^{-1}, linear heating rate of 10 °C min^{-1}.

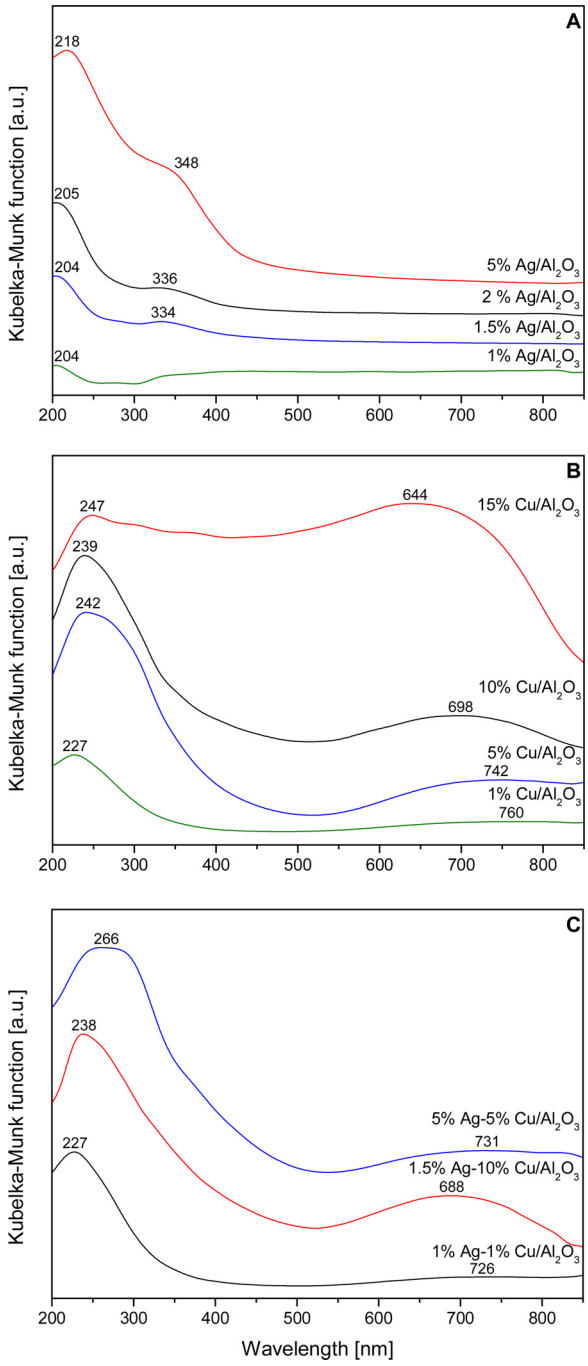

Fig. 3. UV-VIS-DR spectra of Ag/Al_2O_3 (A), Cu/Al_2O_3 (B), $Ag\text{-}Cu/Al_2O_3$ (C).

Ag-10% Cu/Al_2O_3) revealed a lower reduction temperature of the easily reducible CuO_x at about 213 °C. The peak caused by bulk copper oxides species (CuO and $CuAl_2O_4$) shifted to 292–295 °C for both samples, so temperatures lower by about 8–11 °C compared to Cu/Al_2O_3 (303 °C). Moreover, in the H_2-TPR profiles of such Ag-Cu bimetallic systems small peaks centered at around 247–248 °C appeared, which represented a partial reduction of bulk copper oxide species.

UV–vis-DRS analysis allowed insight regarding the type of transition metal species and their aggregation in the Ag-Cu-based materials. In Fig. 3A, a band centered at 204–205 nm for Ag-containing samples (≤2%) is attributed to highly dispersed Ag_2O [21,22]. This band grew in intensity and shifted to higher wavelength (218 nm) for samples with 5% of Ag, indicating a decrease in the dispersion of Ag_2O particles. A shoulder at about 334–336 nm appeared due to oxidized silver clusters $Ag_n^{\delta+}$ [23,24]. Again, for the catalyst containing 5% of silver, the maximum of this peak shifted to higher wavelength. Nevertheless, for all Ag-modified samples, Ag^+ stayed the major Ag species on the Al_2O_3 surface. Fig. 3B shows the UV–vis DR spectra for Cu-containing samples, with two main forms of copper oxide species on the support surface. The peak centered at 227–247 nm can be related to isolated Cu^{2+}, while the absorption at 400–650 nm and above 650 nm arose due to the presence of bulk CuO_x and $CuAl_2O_4$, respectively [14,18]. Again, a higher concentration of copper led to a stronger band corresponding to bulk copper oxide species, well in line with the results of XRD and H_2-TPR analyses. Furthermore, spectra recorded for Ag-Cu bimetallic systems, due to the low loading of Ag, revealed mainly bands related to copper oxide species, as shown in Fig. 3C.

XPS measurements were carried out to further examine the oxidation state of transition metal species in the Ag-Cu-based materials. Fig. 4A–K presents the Ag and Cu XPS spectra, while Table 2 gathers the position of binding energies, full width at half-maxima (FWHM), and molar ratios of the selected Ag-Cu-based materials. The Ag $3d_{5/2}$ binding energies for metallic Ag, Ag_2O and AgO are approximately 368.0–368.3, 367.6–367.8 and 367.3–367.4 eV, respectively [*e.g.* [25–27]. The Ag $3d_{5/2}$ binding energy values of the Ag/Al_2O_3 materials ranged from 368.8 to 367.8 eV for 1 and 5% of Ag, respectively. However, sample characterization by XRD, UV–vis-DRS and H_2-TPR analyses revealed that silver species deposited on the Al_2O_3 surface existed mainly in the form of Ag^+. Furthermore, the binding energy of the highly dispersed silver oxide species was higher than of the Ag_2O clusters (368.8 and 367.8 eV for 1 and 5% of Ag, respectively). Also, in those spectra additional shoulders possibly related to the oxidized silver clusters $Ag_n^{\delta+}$ appeared at 365.1 and 364.7 eV for 1.5 and 5% of silver, respectively. The degrees of support coverage, which are proportional to metal dispersion were calculated using the relative areas of the XPS peaks and normalized by the metal loadings. The results in Table 2 indicated that with the silver loading from 1 to 1.5%, the metal dispersion increased from 0.25 to 0.33, and then subsequently decreased to 0.20 for 5% Ag/Al_2O_3. Fig. 4D–G contains XPS spectra for the Ag 3d states in the selected Ag-Cu bimetallic systems. The binding energy changed with the Ag/Cu ratios in the bimetallic materials, indicating an interaction between silver and copper oxide species. For the bimetallic system with 1% of silver and copper, the binding energy for Ag $3d_{5/2}$ shifted to a lower value (368.8 → 368.1 eV), and became slightly broader with a full width at half maximum (FWHM) from 3.4 to 3.5 eV. Additionally, the Cu 2p peak appeared at 932.5 eV, as reported for Cu^+. Thus, the presence of Cu^+ species on the surface of 1% Cu/Al_2O_3 indicated the reduction of highly dispersed copper oxide species under vacuum. The copper oxide species (CuO_x and $CuAl_2O_4$) were characterized by the appearance of characteristic satellite peaks [26,27]. The other tested bimetallic catalysts with higher copper loading showed Cu^{2+}, as indicated by the shift of peaks to higher binding energies and the appearance of characteristic satellite peaks at 963–962 and 943–942 eV. The comparison of 1% Ag–10% Cu/Al_2O_3 and 1.5% Ag–10% Cu/Al_2O_3 revealed that the addition of silver improved the metal dispersion from 0.37 to 0.40, respectively.

XAFS analyses were carried out to further examine the oxidation state of transition metal species and the near-neighbor atomic environment of the silver and copper atoms in those selected Ag-Cu-based materials. Fig. 5A presents XANES around Ag K-edge of selected Ag-Cu-based materials together with those of Ag foil and Ag_2O. XANES spectra of 1% Ag-1% Cu/Al_2O_3 and 1.5% Ag-10% Cu/Al_2O_3 exhibited similar edge position (at 50% of the height of the rising absorption edge) to that of Ag_2O, which suggested that Ag^+ was the main silver species in bimetallic materials. Furthermore, Fig. 5C–F show raw $k^3\chi(k)$ EXAFS data and Fourier transform of k^3-weighted EXAFS spectra of both Ag-Cu/Al_2O_3, while Table 3 presents the results of the curve-fitting analysis for the first coordination shell. Although the spectra were noisy, a reasonable first shell fit to the data were derived. Both bimetallic materials were similar to each other with regard to the Ag-O and Ag-Ag

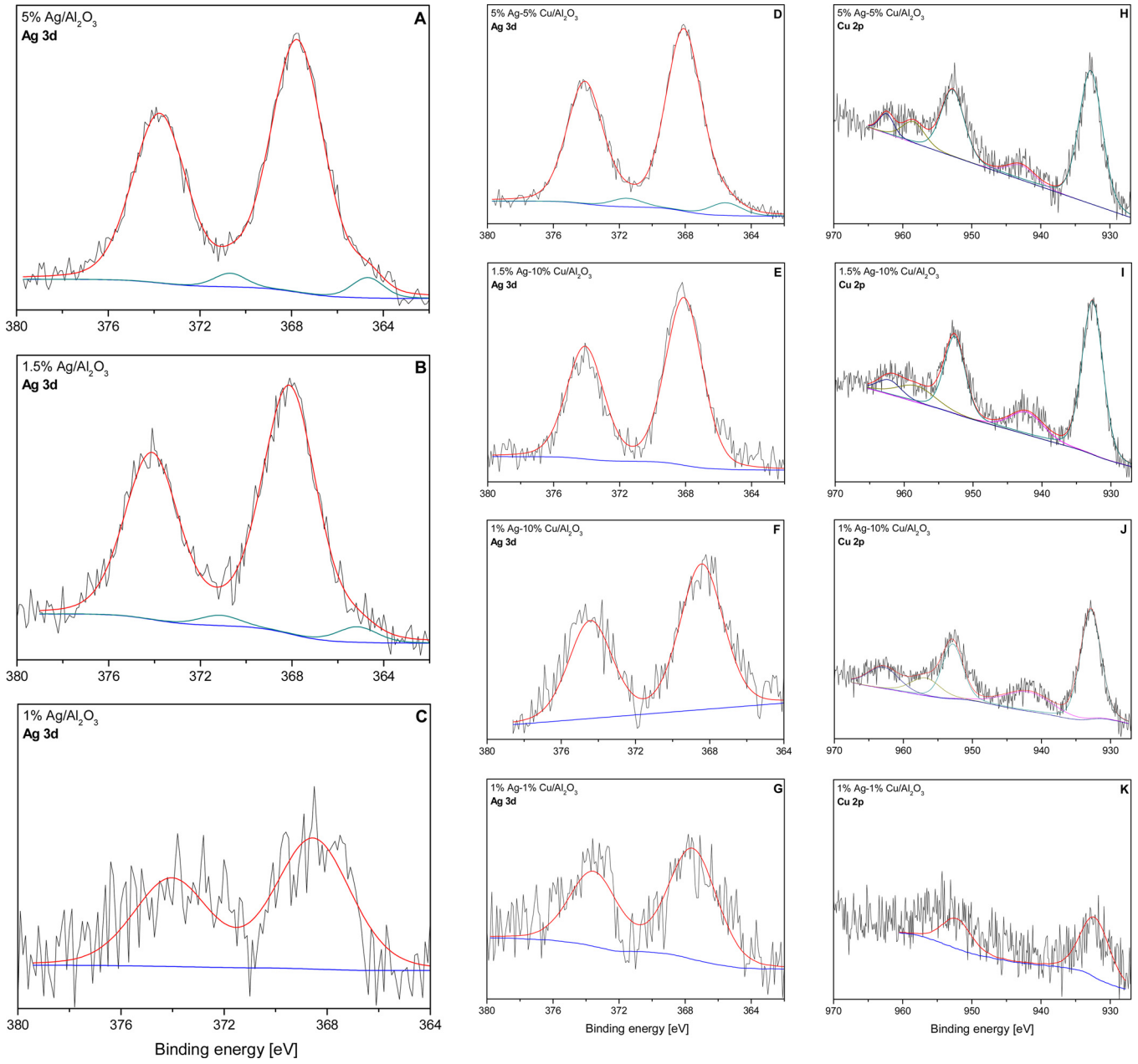

Fig. 4. XP spectra of Ag/Al_2O_3 (A–C) and $Ag\text{-}Cu/Al_2O_3$ (D–K): Ag 3d XPS spectra (A–G) and Cu 2p XPS spectra (H–K).

bond length of 0.226 and 0.276 nm, respectively, consistent with the presence of small silver clusters thought to be up to ~4 silver atoms [28,29]. The slightly larger Ag-O and Ag-Ag coordination numbers seen in 1.5% Ag-10% Cu/Al_2O_3 than those seen in 1% Ag-1% Cu/Al_2O_3 suggested slightly larger silver clusters in the former sample. Furthermore, Fig. 5B shows XANES around Cu K-edge of the selected Ag-Cu-based materials and CuO as reference. The comparison between the edge position of CuO and for both $Ag\text{-}Cu/Al_2O_3$ samples revealed that the investigated materials contained essentially Cu^{2+}. The differences in the rising adsorption edge and XANES region (~50 eV above E0) suggested slight differences in the Cu environment. Based on previous XANES studies of Cu^{2+} the first coordination sphere of the Cu^{2+} environment in 1% Ag-1% Cu/Al_2O_3 and CuO were broadly similar but the second coordination number/sphere was greater in CuO. The XANES spectrum for 1.5% Ag-10% Cu/Al_2O_3 in contrast indicated a very different Cu^{2+} environment. A plot of the Fourier transformed k^3-weighted EXAFS spectra (Fig. 5G) and accompanying EXAFS analysis (results shown in Table 3) confirmed the presence of comparatively isolated Cu^{2+} species in 1% Ag-1% Cu/Al_2O_3 [30]. Analysis of the XANES derivative plots in Fig. 5H suggested the major Cu containing phase in 1.5% Ag-10% Cu/Al_2O_3 to be $CuAl_2O_4$ [31]. However, XRD, H_2-TPR, UV–vis-DRS and XPS analyses revealed a mixture of CuO and $CuAl_2O_4$ formed in Cu-containing catalysts.

The catalytic results of the selective ammonia oxidation into nitrogen and water vapour (NH_3-SCO) provided insight into activity and selectivity of silver and/or copper species in the Ag-Cu-based materials. The γ-Al_2O_3 support was almost inactive in the investigated temperature range [18]. Fig. 6 shows the results of NH_3-SCO of Ag-Cu-based catalysts, while Table 4 gathers temperatures for which 50% (T_{50}) and full conversions (T_{100}) were achieved for tested catalysts together with selectivity to particular products at these temperatures. The catalytic activity increased gradually with increasing silver loading (Fig. 6A–D). Ag/Al_2O_3 doped with 1% of silver reached full conversion at a temperature as high as 500 °C. Significantly higher activity and selectivity were obtained over the 1.5–2% Ag/Al_2O_3 catalysts with full ammonia conversion at 300–325 °C and 84% N_2 selectivity. Even higher activity

Table 2
Position of binding energies, full width at half-maxima (FWHM) and molar ratios of Ag/Al_2O_3 and $Ag\text{-}Cu/Al_2O_3$.

Sample code	Peak Position/FWHM [eV]			Molar ratio[a] Ag 3d/Al 2p*
	Ag 3d	O 1s	Cu 2p	(Ag 3d + Cu 2p)/Al 2p**
1% Ag/Al_2O_3	368.8/3.4	532.5/2.1 531.1/2.1 529.8/2.3		0.25*
1.5% Ag/Al_2O_3	368.1/2.8 365.1/2.1	532.5/2.4 530.9/2.5 528.9/2.6		0.33*
5% Ag/Al_2O_3	367.8/2.8 364.7/1.6	532.7/2.0 530.9/2.4 529.3/2.4		0.20*
1% Ag-1% Cu/Al_2O_3	368.1/3.5	532.1/2.5 530.7/2.2 529.3/2.4	932.5/5.0	0.61**
1% Ag-10% Cu/Al_2O_3	368.4/2.8	532.5/2.3 530.9/2.5 529.3/2.4	962.9/5.3 956.8/5.1 941.9/8.2 932.9/3.5	0.37**
1.5% Ag-10% Cu/Al_2O_3	368.1/2.6	532.4/2.6 530.9/2.6 529.3/2.5	962.2/4.0 958.2/6.5 942.2/5.7 932.7/3.6	0.40**
5% Ag-5% Cu/Al_2O_3	368.1/2.6 365.5/2.2	532.5/2.1 530.9/2.5 529.4/2.4	962.3/2.5 958.4/3.9 942.9/4.6 932.8/3.9	0.43**

[a] Estimated from the integrated areas of the respective XPS peaks and normalized by metal loading.

was achieved over catalysts containing 5% of silver. However, the selectivity to N_2 decreased to an unsatisfying level of 57% at 400 °C, and then started increasing again possibly due to an increasing contribution of Ag_2O clusters with lower reducibility (Fig. 2A). The significant amounts of by-products produced in the presence of 5% Ag/Al_2O_3 excluded such catalysts from the application in NH_3-SCO. The results above clearly showed that silver-containing catalysts were active for ammonia oxidation, and superior to Cu-modified Al_2O_3. In particular, for a material containing 1% of copper, full conversion of ammonia from the reaction mixture was not reached up to 500 °C. Similarly to the Ag/Al_2O_3 catalysts, the activity of Cu-doped materials significantly increased with increasing amount of transition metal. Though further variation of the copper loading from 5 to 15% did not result in a significantly different activity. For catalysts with 10–15% of copper, full ammonia conversion was reached at 425 °C. While the selectivity to N_2 decreased with increasing amount of copper, possibly due to an increasing amount of bulk CuO_x and $CuAl_2O_4$ on the catalyst surfaces (Fig. 2B). Similarly, Jabłońska et al. [32] reported gradual decrease in N_2 selectivity up to 500 °C over Cu-Mg-Al mixed oxides containing bulk CuO_x and $CuAl_2O_4$.

For further catalyst optimization, Al_2O_3 was modified simultaneously with silver and copper, as shown on Fig. 6I–L. Among all tested combinations – 1–1, 1–10, 1.5–10, 5–5% of silver and copper, respectively – 1.5% Ag-10% Cu/Al_2O_3 reached an optimum ammonia conversion at 375 °C and 94% N_2 selectivity at this temperature. Noteworthy, the activity of this catalyst did not change significantly in NH_3-SCO under wet conditions (3.2% of water vapour). The activity of this sample under wet conditions shifted by 50 °C to higher temperature, while the selectivities to all products remained nearly constant. A stability test for 1.5% Ag-10% Cu/Al_2O_3 (Fig. 6P) was carried out at 325 °C over a feed containing besides NH_3 and O_2, also water vapour. The catalyst allowed a conversion of 76% with a N_2 selectivity of 97%, after 500 min time on stream. Ag-Cu-modified Al_2O_3 (Ag-Cu: 7.5–2.5, 5–5, 10–10%) were studied before but only in the temperature range of 350–400 °C by Gang et al. [8] and Yang et al. [5]. Among the tested catalysts, 7.5% Ag-2.5% Cu/Al_2O_3 facilitated complete ammonia conversion at 300 °C with 95% N_2 selectivity. Above 300 °C more by-products appeared. An increase in silver loading resulted in activation of the catalyst, but caused also an increasing NO_x and N_2O formation [8]. Thus, the activity and selectivity of NH_3-SCO over Ag-Cu/Al_2O_3 catalysts strongly depends on the transition metal loadings. Our results emphasize that the activity and selectivity to N_2 can be steered into the desired direction by a co-impregnation of proper amounts of silver and copper on the Al_2O_3 support. Accordingly, the selectivity to by-products were clearly suppressed.

Temperature programmed desorption (NH_3-TPD) and temperature programmed surface reaction (NH_3-TPSR) were carried out to investigate the ammonia adsorption and the surface reaction between adsorbed ammonia and oxygen. Fig. 7A presents NH_3 temperature programmed desorption profiles for 1.5% Ag/Al_2O_3. NH_3 desorbed from this catalyst over a broad range of temperatures covering 70–450 °C. Apart from ammonia, reaction products – N_2, NO and N_2O – were detected at temperatures from 70 to 500 °C. N_2O as the first reaction product appeared at around 250 °C. N_2 appeared at higher temperatures (> 400 °C), while NO was not detected during this experiment. Thus, NH_3 could be oxidized over lattice oxygen of Ag_xO to a limited extent, and N_2O was the main product at 250–450 °C. Furthermore, Fig. 7B shows NH_3 temperature programmed surface reaction profiles over Ag/Al_2O_3. NH_3 desorbed mainly at low temperatures (< 250 °C), indicating a high NH_3 oxidation efficiency of Ag/Al_2O_3. N_2 was the main reaction product in the range of 70–250 °C, while N_2O appeared in two broad stages: 70–250 and 250–500 °C. A minor amount of NO was detected over Ag/Al_2O_3 above 350 °C during NH_3-TPSR. Thus, the adsorbed NH_3 reacted mainly with the gas-phase O_2 over Ag/Al_2O_3 yielding the reaction products: N_2, N_2O and NO. Fig. 7C presents the NH_3-TPD profile of Cu/Al_2O_3. NH_3 was desorbed over such catalyst up to 350 °C, with N_2 as the main reaction product in the range of 200–400 °C. Besides N_2, by-products were also detected: N_2O above

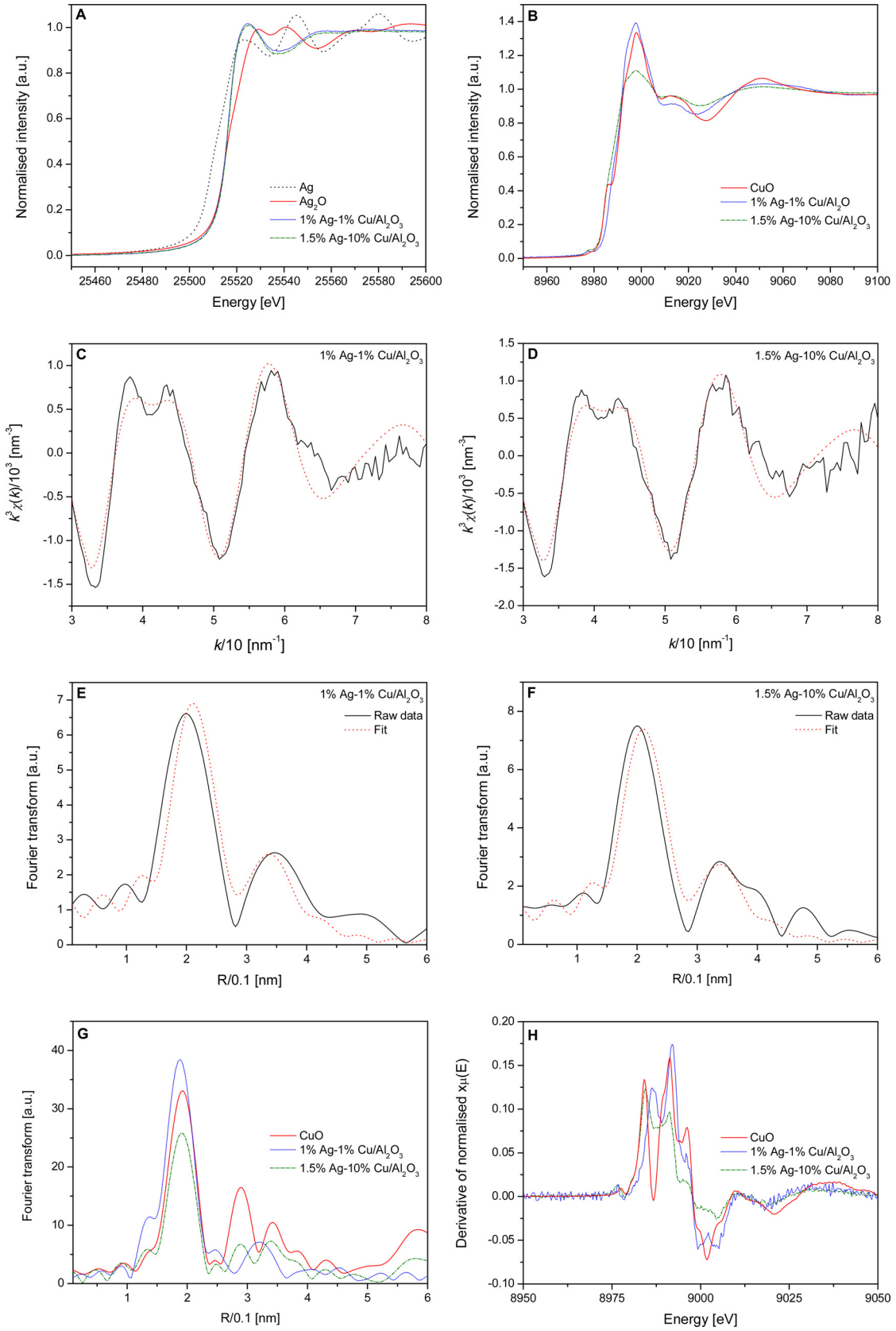

Fig. 5. Ag K-edge (A) and Cu K-edge (B) XANES spectra, raw$k^3\chi(k)$ EXAFS data (C,D), fourier transform of k^3-weighted EXAFS spectra (E–G), and derivative of the normalized X-ray absorption (H) of 1% Ag-1% Cu/Al_2O_3 and 1.5% Ag-10% Cu/Al_2O_3 (and references (Ag, Ag_2O, CuO).

Table 3
Coordination numbers (CN), bond distances between adsorbed and backscatter atoms (R), inner potential correction to account for the difference in the inner potential between the sample and the reference compound (E), Debye-Waller factors ($2\sigma^2$), and residual factors (R) of 1% Ag-1% Cu/Al_2O_3 and 1.5%Ag-10%Cu/Al_2O_3.

Sample code	Shell	CN	R [nm]	E [eV]	$2\sigma^2$	R [%]
1% Ag-1% Cu/Al_2O_3	Ag-O	1.9	0.226	−0.47	0.027	32
	Ag-Ag	2.7	0.276		0.062	
	Cu-O	4	0.195	−0.55	0.018	31
	Cu-Cu	2.7	0.305		0.04	
1.5% Ag-10% Cu/Al_2O_3	Ag-O	2	0.226	−2.3	0.027	30.3
	Ag-Ag	2.9	0.276		0.062	

150 °C and NO above 375 °C, respectively. Thus, NH_3 was partially oxidized by lattice oxygen of copper oxide species under these conditions. During the NH_3-TPSR performed for ammonia desorption in the presence of O_2, N_2 appeared in the range of 200–350 °C. While significant amounts of N_2O and NO were detected above 150 and 350 °C, respectively, as presented in Fig. 7D. Again, NH_3 reacted mainly with lattice oxygen of the catalyst, which was supplied under O_2 atmosphere.

Furthermore, Fig. 7E and F illustrate NH_3-TPD and NH_3-TPSR for 1.5% Ag-10% Cu/Al_2O_3. As a result of differences between silver and copper oxide species, the profiles of NH_3 desorption and reaction products' evolution varied appreciably during both experiments over the bimetallic sample. In particular, during NH_3-TPD of Ag-Cu/Al_2O_3, the lattice oxygen of copper oxide species partially oxidised adsorbed ammonia, yielding N_2 as the main reaction product in the range of 200–400 °C. N_2O was a minor product above 150 °C with a maximum in the range of 150–300 °C. While NO was not detected over Ag-Cu/Al_2O_3. During NH_3-TPSR, a significant amount of NO appeared in the high temperature range (above 350 °C). Thus, the interaction between silver and copper oxide species played an important role in NH_3 activation and its oxidation. The silver oxide species enhanced low temperature activity of NH_3 oxidation mainly into N_2 (< 250 °C). However, at high temperatures the selectivity to by-products increased. While the copper oxide species facilitated the formation of N_2 at higher temperatures up to 350 °C.

In situ DRIFTS studies were carried out to investigate the role of silver and/or copper oxide species for the adsorption of NH_3 on Ag-Cu-based catalysts. Table 5 summarizes the assignments of the FTIR bands observed upon adsorption of NH_3. In Fig. 8A, the bands at 1687, 1475 and 1396 cm^{-1} appeared due to the deformation modes of NH_4^+ formed by the interaction of NH_3 with Brönsted acid sites on γ-Al_2O_3 [33–37]. The bands at 1622 and 1235 cm^{-1} can be assigned to the asymmetric and symmetric deformation modes, respectively, of NH_3 molecules coordinated on Lewis acid sites of the γ-Al_2O_3 support [33–37]. The two bands – at 1449 cm^{-1} ascribed to the imide (–NH) deformation modes, and at 1350 cm^{-1} ascribed to the amide ($–NH_2$) wagging [38,39] – appeared at 50 °C. Both bands together with the bands from NH_3 coordinated on Brönsted and Lewis acid sites decreased gradually with increasing temperature. The band at 1449 cm^{-1} remained stable until 300 °C, while the band at 1350 cm^{-1} disappeared above 50 °C. At about 300 °C, the peak related to the amide ($-NH_2$) scissoring gradually increased at 1580 cm^{-1}. Thus, NH_3 adsorbed on Ag/Al_2O_3 was activated to form $-NH_x$ ($-NH_2$ and −NH) intermediates, which desorbed from the surface of the catalyst. Nevertheless, the band

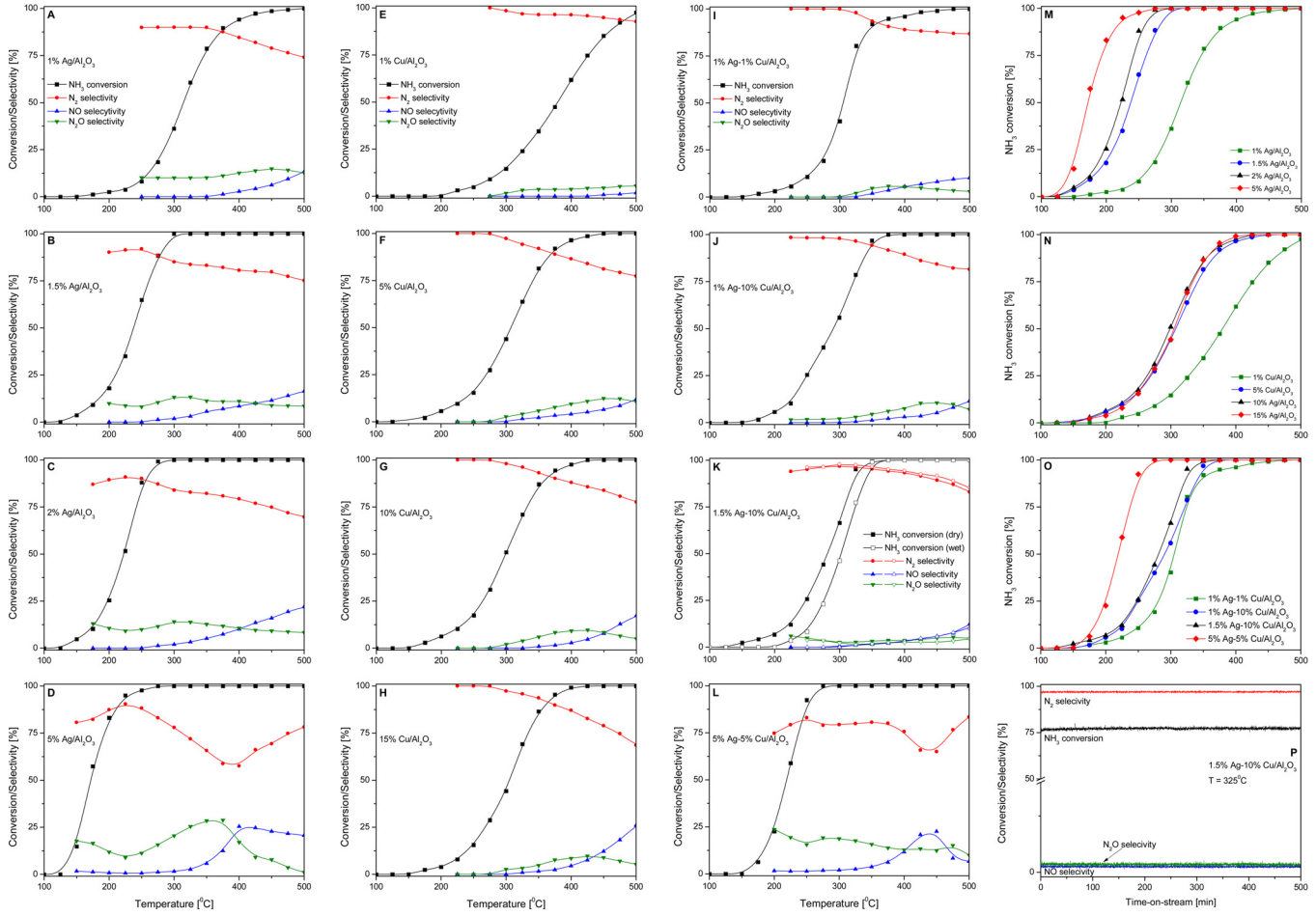

Fig. 6. Results of catalytic tests for NH_3-SCO performed over Ag/Al_2O_3, Cu/Al_2O_3, Ag-Cu/Al_2O_3; experimental conditions: mass of catalyst = 100 mg, [NH_3] = 0.5 vol.%, [O_2] = 2.5 vol.%, ([H_2O] = 3.2 vol.%), Ar balance, total flow rate = 40 ml min^{-1}, linear heating rate of 5 °C min^{-1}.

Table 4
Comparison of the results of catalytic tests (T_{50} and T_{100} temperature needed for 50 and 100% of NH_3 conversion, respectively).

Sample codes	T_{50}, *T_{100} [°C]	N_2 selectivity	NO selectivity at T_{50}, *T_{100} [%]	N_2O selectivity
1% Ag/Al_2O_3	314 *500	90 *74	0 *13	10 *13
1.5% Ag/Al_2O_3	238 *325	92 *84	0 *3	8 *13
2% Ag/Al_2O_3	222 *300	90 *84	0 *2	10 *14
5% Ag/Al_2O_3	172 *275	83 *83	1 *1	16 *16
1% Cu/Al_2O_3	379 *-	96 *-	0 *-	*4 –
5% Cu/Al_2O_3	308 *450	96 *81	*1 7	*3 12
10% Cu/Al_2O_3	299 *425	98 *85	0 *5	2 *10
15% Cu/Al_2O_3	305 *425	97 *83	0 *7	3 *10
1% Ag-1% Cu/Al_2O_3	305 *475	99 *87	0 *10	1 *3
1% Ag-10%Cu/Al_2O_3	290 *375	98 *92	0 *2	2 *6
1.5% Ag-10% Cu/Al_2O_3*	281 *375	97 *94	0 *2	3 *4
*with 3.2% H_2O	302 *375	98 *95	0 *2	2 *3
5% Ag-5% Cu/Al_2O_3	219 *275	78 *79	2 *2	20 *19

Table 5
Assignments of the FTIR bands.

Wavenumber [cm^{-1}]	Surface species	Refs.
1691–1684 1481–1475 1403–1396	NH_4^+	[33–37]
1629–1619 1261–1235	NH_3L	[33–37]
1450–1449 1350 1583-1580	–NH –NH_2 wagging –NH_2 scissoring	[38,39]
	bidentate nitrates	[40]
1652–1651	bridging nitrate	[43]
1558–1553 1540–1539 1463, 1403	bidentate nitrate monodentate nitrate chelating nitro	
1330–1326	free NO_2^- ion	[42]

located at 1580 cm^{-1} could arise due to bidentate nitrates [40]; however, in the NH_3-TPD profile for Ag/Al_2O_3 (Fig. 7A), we did not observe NO_x produced in the studied temperature range of 70–500 °C. In the N—H stretching region a broad band ranging from 3350 to 3100 cm^{-1} occurred [38,39,41]. Furthermore, the NH_3-SCO mechanism was studied with respect to the behavior of adsorbed NH_3 species interacting with O_2 on the surface of Ag/Al_2O_3. Fig. 8B presents the *in situ* FTIR spectra of Ag/Al_2O_3 at various temperatures (50–350 °C). The bands of NH_3 coordinated to Brönsted acid sites appeared at 1691, 1475 and 1393 cm^{-1}, while the bands coordinated to Lewis acid sites existed at 1622 and 1243 cm^{-1}. Band of —NH and —NH_2 appeared at 50 °C at 1449 and 1350 cm^{-1}, respectively, and their intensity slightly increased with increasing temperature. Above 100 °C, a band corresponding to —NH_2 appeared at 1580 cm^{-1} and strongly increased up to 350 °C. The band at 1580 cm^{-1} could be attributed to bidentate nitrate, because NO was formed above 350 °C over Ag/Al_2O_3 in the presence of gaseous O_2 as indicated by the NH_3-TPSR results (Fig. 7B). Additionally, new bands at 1652 cm^{-1} (at about 250 °C), at 1463 cm^{-1} (at about

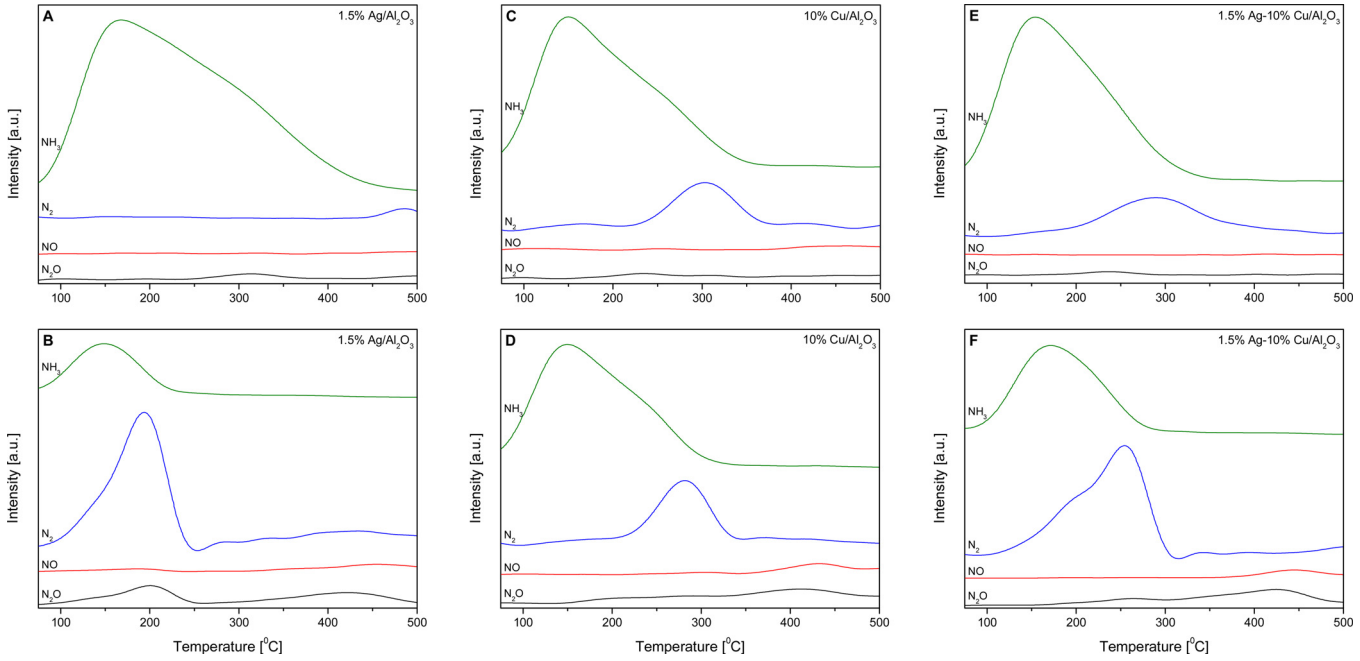

Fig. 7. Results of NH_3-TPD (A,C,E) and NH_3-TPSR (B, D and F) for Ag/Al_2O_3 (A and B), Cu/Al_2O_3 (C and D), Ag-Cu/Al_2O_3 (E and F); experimental conditions: mass of catalyst = 100 mg, adsorption: 70 °C, [NH_3] = 1 vol.%, Ar balance, total flow rate = 20 ml min^{-1}; desorption: 70–500 °C, pure argon (NH_3-TPD) or [O_2] = 5 vol.%, Ar balance (NH_3-TPSR), total flow rate = 20 ml min^{-1}, linear heating rate of 5 °C min^{-1}.

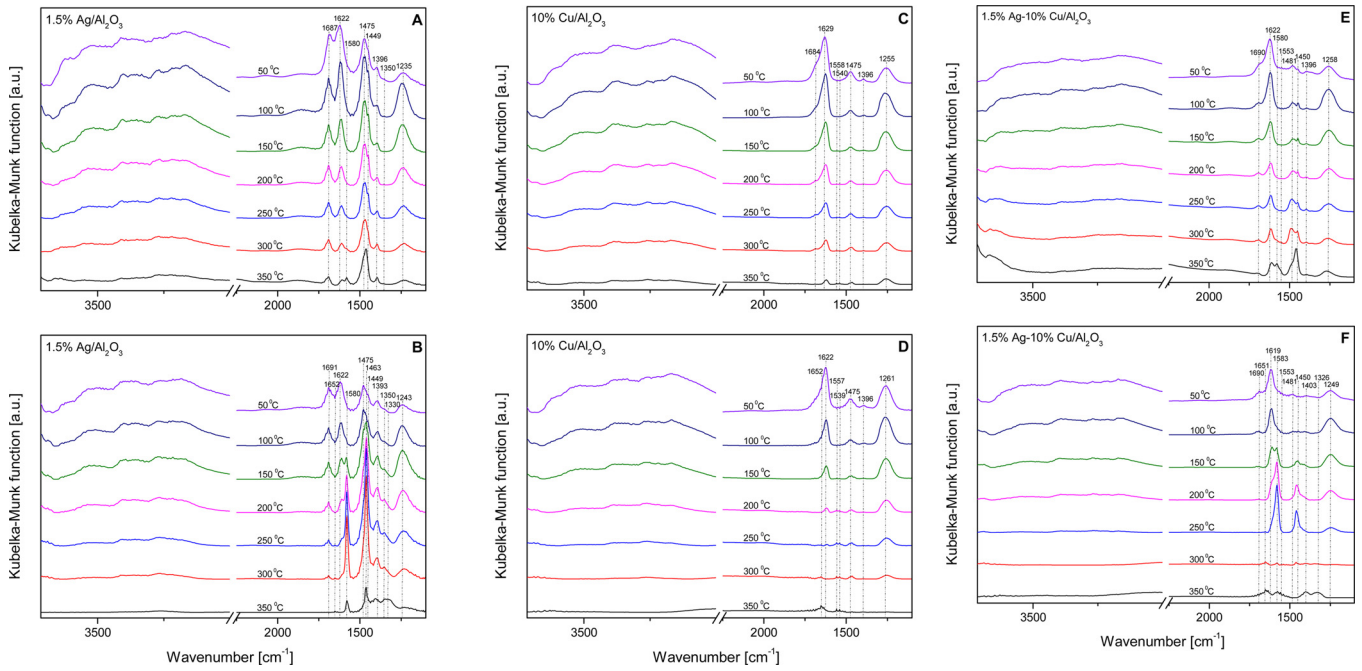

Fig. 8. *In situ* DRIFTS spectra of the adsorbed species arising from contact with NH_3 with Ag/Al_2O_3 (A and B), Cu/Al_2O_3 (C,D), $Ag\text{-}Cu/Al_2O_3$ (E,F) at 50 °C and successive purging with N_2 (A, C and E), or $[O_2]$ = 5 vol.%, Ar balance (B,D,F) at 50–350 °C.

150 °C) and at 1330 cm^{-1} (at about 350 °C), appeared also due to bridging nitrate, chelating nitro and free NO_2^- ions [42], respectively. Thus, the adsorbed NH_x was mainly oxidized by gas-phase O_2, and adsorbed as nitrites/nitrates on the Ag/Al_2O_3 catalyst in the presence of O_2. While the reaction between NO and excessive hydrogen abstraction of NH_3, *i.e.* NH_x species, yielded N_2 and N_2O (Fig. 7B). The FTIR bands observed upon adsorption of NH_3 on Ag/Al_2O_3 after successive purging in N_2 appeared also in the spectra of Cu/Al_2O_3 (NH_3 coordinated on (i) Brönsted acid sites: 1684, 1475 and 1396 cm^{-1}; (ii) Lewis acid sites: 1629 and 1255 cm^{-1}; Fig. 8C) and $Ag\text{-}Cu/Al_2O_3$ (i): 1690, 1481 and 1396 cm^{-1}; (ii): 1622 and 1258 cm^{-1}; Fig. 8E). NH_3 adsorbed mainly on Brönsted and Lewis acid sites, however, these bands showed different intensity on the $M\text{-}Al_2O_3$ (M = Ag, Cu, or Ag-Cu) catalysts. Cu/Al_2O_3 revealed relatively low intensity of the bands corresponding to NH_3 coordinated to Brönsted acid sites. Additionally, small bands appeared above 150 °C for Cu/Al_2O_3 at 1558 and 1540 cm^{-1}, while for $Ag\text{-}Cu/Al_2O_3$, at 1553 cm^{-1}, which were assigned to the bidentate (1558–1553 cm^{-1}) and monodentate nitrates (1540 cm^{-1}) [43]. Thus, in the absence of O_2, adsorbed ammonia was oxidised by lattice oxygen (O_2^-) of copper oxide species with formation of NO_x ad-species. Such *in situ* formed NO_x ad-species possibly reacted with adsorbed NH_3 yielding N_2 and N_2O (Fig. 7C and E). In the presence of gaseous O_2 (i) Brönsted acid sites: 1652, 1475 and 1396 cm^{-1}; (ii) Lewis acid sites: 1622 and 1261 cm^{-1} over Cu/Al_2O_3; Fig. 8D), and (i): 1690 and 1481 cm^{-1}; (ii): 1619 and 1249 cm^{-1} over $Ag\text{-}Cu/Al_2O_3$; Fig. 8F) were detected. Analogously, other bands attributed to bidentate and monodentate nitrates at 1557 and 1539 cm^{-1}, respectively, appeared in the spectrum of Cu/Al_2O_3 after successive purging in O_2. While the bands assigned to bridging nitrate (1651 cm^{-1}), chelating nitro (1403 cm^{-1}) and free NO_2^- ion (1326 cm^{-1}) appeared in the spectrum of $Ag\text{-}Cu/Al_2O_3$. The formation of these three species over $Ag\text{-}Cu/Al_2O_3$ was strongly enhanced by the presence of gas-phase O_2. Moreover, the spectrum of $Ag\text{-}Cu/Al_2O_3$ contained bands detected also for Ag/Al_2O_3 (−NH at 1450 cm^{-1}, $-NH_2$ scissoring or bidentate nitrates at 1583 cm^{-1}) and for Cu/Al_2O_3 (bidentate nitrates at 1553 cm^{-1}) species. Thus, the presence of silver oxide species enhanced dehydrogenation of chemisorbed NH_3 molecules much faster than copper oxide species, and therefore a significant population of $NH_{3\text{-}x}$ (x = 1,2) species appeared on the Ag/Al_2O_3 and $Ag\text{-}Cu/Al_2O_3$ surfaces.

Based on the above *in situ* FTIR results, adsorbed NH_3 was activated through hydrogen abstraction over Ag/Al_2O_3, and further partially oxidized by gas-phase O_2 to bridging nitrate, chelating nitro and free NO_2^- ions, finally yielding N_2 and N_2O. Moreover, adsorbed NH_3 – as protonated NH_4^+ on Brönsted acid sites and coordinated NH_3 on Lewis acid sites – was oxidized to bidentate and monodentate nitrates over lattice oxygen of copper oxide species of Cu/Al_2O_3. In the presence of gas-phase O_2, the evolution of NO was observed only in the high temperature range (Fig. 7B, D and F). At these temperatures no chemisorbed ammonia was converting *in situ* formed NO_x ad-species to N_2 and N_2O. Therefore, we concluded that NH_3-SCO on the Ag/Al_2O_3, Cu/Al_2O_3 and $Ag\text{-}Cu/Al_2O_3$ followed an *in situ* selective catalytic reduction (i-SCR) mechanism, which involved the partial oxidation of NH_3 into NO_x species, along with adsorbed NO_x species interacting with NH_x and being reduced to reaction products. Ag_2O was an active species for the activation of NH_3, followed by its partial oxidation by gaseous O_2 into NO_x species. Otherwise, a significant amount of desorbed NH_3 for Cu/Al_2O_3 (Fig. 7D), suggested that the majority of chemisorb ammonia was not involved in the low temperature oxidation. Thus, chemisorb ammonia on CuO_x played a role of NO_x reducer below 350 °C. Consequently, the $Ag\text{-}Cu/Al_2O_3$ catalyst–containing both metal oxide species, revealed optimized activity and N_2 selectivity in NH_3-SCO.

In situ formed NO_x were the main intermediates of this mechanism. We could not exclud that an interaction between the NH_3 and *in situ* formed NO_x ad-species led to formation of NH_2NO, NH_2NO_2 or NH_2NO_3 intermediate species with low thermal stability, which easily decomposed into N_2 with N_2O as a by-product [41]. Noteworthy, the results of NH_3-TPD or NH_3-TPSR did not reveal the evolution of NO_2, indicating NO as the main reaction intermediate. Nevertheless, the detailed recognition of an i-SCR pathway needs additional studies, *e.g. in situ* DRIFT studies of interaction of NH_3 with *in situ* formed NO_x ad-species

[44,45], as well as *in situ* DRIFTS coupled with transient techniques (TAP, SSITKA) in order to provide information on the surface coverage of active and inactive (spectators) species under reaction conditions. Such experiments will be investigated separately.

4. Conclusion

We investigated the influence of different loadings of Ag and/or Cu – Ag (1–5%), Cu (10–15%) or Ag-Cu (1–1, 1–10, 1.5–10, 5–5% of metal) on the physicochemical properties, catalytic activity and selectivity in NH_3-SCO. XRD, H_2-TPR, UV–vis-DRS, XPS and EXAFS analyses revealed that silver species existed mainly in the form of Ag_2O, while copper oxide species coexisted as CuO and $CuAl_2O_4$ on Ag/Al_2O_3, Cu/Al_2O_3 and $Ag\text{-}Cu/Al_2O_3$ surfaces, respectively. Silver species significantly decreased the temperature of the ammonia oxidation but also decreased the selectivity to N_2 with increasing silver loading up to 5%. Copper oxide species were significantly less active in the ammonia oxidation, but more selective to N_2. Easily reducible highly dispersed CuO_x promoted the activity of 5–15% Cu/Al_2O_3, while bulk CuO_x and $CuAl_2O_4$ decreased N_2 selectivity up to 500 °C. Thus, the activity and selectivity were optimized by tuning the loading of silver and copper in $Ag\text{-}Cu/Al_2O_3$. We selected 1.5% Ag-10% Cu/Al_2O_3 as promising catalyst for NH_3-SCO, which operated at relatively low temperature with high selectivity to N_2 (full NH_3 conversion at 375 °C with 94% N_2 selectivity). NH_3-TPD, NH_3-TPSR and *in situ* FTIR measurements confirmed the *in situ* selective catalytic reduction (i-SCR) mechanism over 1.5% Ag/Al_2O_3, 10% Cu/Al_2O_3 and 1.5% Ag-10% Cu/Al_2O_3. However, copper oxide species were less active in ammonia oxidation than silver oxide species. Thus, the high activity and N_2 selectivity of $Ag\text{-}Cu/Al_2O_3$ catalyst were assigned to the enhanced activity of silver species in ammonia oxidation to NO_x and activity of copper oxide species in NO_x reduction with unreacted ammonia to N_2 and N_2O.

Acknowledgements

Funded by the Excellence Initiative of the German federal and state governments in the frame of the Center for Automotive Catalytic Systems Aachen (ACA) at RWTH Aachen University and EPSRC (UK). The authors acknowledge the Diamond Light Source (beamtime application SP14834) for provision of beamtime on the beamlines B18, and Diego Gianolio and Miren Agote for assistance in performing the XAFS measurements.

References

[1] Z. Qu, H. Wang, S. Wang, H. Cheng, Y. Qin, Z. Wang, Role of the support on the behavior of Ag-based catalysts for NH_3 selective catalytic oxidation (NH_3-SCO), Appl. Surf. Sci. 316 (2014) 373–379.
[2] L. Zhang, C. Zhang, H. He, The role of silver species on Ag/Al_2O_3catalysts for the selective catalytic oxidation of ammonia to nitrogen, J. Catal. 261 (2009) 101–109.
[3] L. Zhang, F. Liu, Y. Yu, Y. Liu, C. Zhang, H. He, Effects of adding CeO_2 to Ag/Al_2O_3 catalyst for ammonia oxidation at low temperatures, Chin. J. Catal. 32 (2011) 727–735.
[4] L. Gang, B.G. Anderson, J. van Grondelle, R.A. van Santen, Low temperature selective oxidation of ammonia to nitrogen on silver-based catalysts, Appl. Catal. B: Environ. 40 (2003) 101–110.
[5] M. Yang, C. Wu, C. Zhang, H. He, Selective oxidation of ammonia over copper-silver-based catalysts, Catal. Today 90 (2004) 263–267.
[6] M. Jabłońska, R. Palkovits, Copper based catalysts for the selective ammonia oxidation into nitrogen and water vapour-recent trends and open challenges, Appl. Catal. B: Environ. 181 (2016) 332–351.
[7] L. Chmielarz, M. Jabłońska, A. Strumiński, Z. Piwowarska, A. Węgrzyn, S. Witkowski, M. Michalik, Selective catalytic oxidation of ammonia to nitrogen over Mg-Al, Cu-Mg-Al and Fe-Mg-Al mixed metal oxides doped with noble metals, Appl. Catal. B: Environ. 130–131 (2013) 152–162.
[8] L. Gang, B.G. Anderson, J. van Grondelle, R.A. van Santen, W.J.H. van Gennip, J.W. Niemantsverdriet, P.J. Kooyman, A. Knoester, H.H. Brongersma, Alumina-supported Cu–Ag catalysts for ammonia oxidation to nitrogen at low temperature, J. Catal. 206 (2002) 60–70.
[9] M. Newville, IFEFFIT: interactive XAFS analysis and FEFF fitting, J. Synchrotron Radiat. 8 (2001) 322–324.
[10] B. Ravel, M. Newville, Athena, artemis, hephaestus: data analysis for X-ray absorption spectroscopy using IFEFFIT, J. Synchrotron Radiat. 12 (2005) 537–541.
[11] H. Wan, D. Li, Y. Dai, Y. Hu, B. Liu, L. Dong, Catalytic behaviors of CuO supported on Mn_2O_3 modified γ-Al_2O_3 for NO reduction by CO, J. Mol. Catal. A: Chem. 332 (2010) 32–44.
[12] G. Wang, X. Ma, B. Huang, H. Cheng, Z. Wang, J. Zhan, X. Qin, X. Zhang, Y. Dai, Controlled synthesis of Ag_2O microcrystals with facet-dependent photocatalytic activities, J. Mater. Chem. 22 (2012) 21189–21194.
[13] W. Wang, Y. Zhan, G. Wang, One-step, solid-state reaction to the synthesis of copper oxide nanorods in the presence of a suitable surfactant, Chem. Commun. (2001) 727–728.
[14] C. Liang, X. Li, Z. Qu, M. Tade, S. Liu, The role of copper species on Cu/γ-Al_2O_3 catalysts for NH_3-SCO reaction, Appl. Surf. Sci. 258 (2012) 3738–3743.
[15] M. Luo, X. Yuan, X. Zheng, Catalyst characterization and activity of Ag-Mn, Ag-Co and Ag–Ce composite oxides for oxidation of volatile organic compounds, Appl. Catal. A: Gen. 175 (1998) 121–129.
[16] A. Musi, P. Massiani, D. Brouri, J.-M. Trichard, P. Da Costa, On the characterisation of silver species for SCR of NO_x with ethanol, Catal. Lett. 128 (2009) 25–30.
[17] M. Jabłońska, M. Nocuń, E. Bidzińska, Silver-alumina catalysts for low-temperature methanol incineration, Catal. Lett. 146 (2016) 937–944.
[18] M. Jabłońska, Selective catalytic oxidation of ammonia into nitrogen and water vapour over transition metals modified Al_2O_3, TiO_2 and ZrO_2, Chem. Pap. 69 (2015) 1141–1155.
[19] B.R. Strohmeier, D.E. Levden, R.S. Field, D.M. Hercules, Surface spectroscopic characterization of $CuAl_2O_3$ catalysts, J. Catal. 94 (1985) 514–530.
[20] L. Jin, M. He, J. Lu, M. Luo, P. Fang, Y. Xie, Comparative study of CuO species on CuO/Al_2O_3, CuO/CeO_2-Al_2O_3 and CuO/La_2O-Al_2O_3 catalysts for CO oxidation, Chin. J. Chem. Phys. 20 (2007).
[21] J. Lu, J.J. Bravo-Suárez, M. Haruta, S.T. Oyama, Direct propylene epoxidation over modified $Ag/CaCO_3$ catalysts, Appl. Catal. A: Gen. 302 (2006) 283–295.
[22] N. Bogdanchikova, F.C. Meunier, M. Avalos-Borja, J.P. Breen, A. Pestryakov, On the nature of the silver phases of Ag/Al_2O_3 catalysts for reactions involving nitric oxide, Appl. Catal. B: Environ. 36 (2002) 287–297.
[23] A. Keshavaraja, X. She, M. Flytzani-Stephanopoulos, Selective catalytic reduction of NO with methane over Ag-alumina catalysts, Appl. Catal. B: Environ. 27 (2000) L1–L9.
[24] X. She, M. Flytzani-Stephanopoulos, The role of AgOAl species in silver–alumina catalysts for the selective catalytic reduction of NO_x with methane, J. Catal. 237 (2006) 79–93.
[25] Y. Lai, H. Zhuang, K. Xie, D. Gong, Y. Tang, L. Sun, C. Lin, Z. Chen, Fabrication of uniform Ag/TiO_2 nanotube array structures with enhanced photoelectrochemical performance, N. J. Chem. 34 (2010) 1335–1340.
[26] E. Sumesh, M.S. Bootharaju, T. Anshup, Pradeep, A practical silver nanoparticle-based adsorbent for the removal of Hg^{2+} from water, J. Hazard. Mater. 189 (2011) 450–457.
[27] F. Xiao, H.-G. Liu, Y.-I. Lee, Formation and characterization of two-dimensional arrays of silver oxide nanoparticles under Langmuir monolayers of n-hexadecyl dihydrogen phosphate, Bull. Korean Chem. Soc. 29 (2008) 2368–2372.
[28] J. Shibata, K. Shimizu, Y. Takada, A. Shichi, H. Yoshida, S. Satokawa, A. Satsuma, T. Hattori, Structure of active Ag clusters in Ag zeolites for SCR of NO by propane in the presence of hydrogen, J. Catal. 227 (2004) 367–374.
[29] S.T. Korhonen, A.M. Beale, M.A. Newton, B.M. Weckhuysen, New insights into the active surface species of silver alumina catalysts in the selective catalytic reduction of NO, J. Phys. Chem. C 115 (2011) 885–896.
[30] I. Lezcano-Gonzalez, U. Deka, H.E. van der Bij, P. Paalanen, B. Arstad, B.M. Weckhuysen, A.M. Beale, Chemical deactivation of Cu-SSZ-13 ammonia selective catalytic reduction (NH_3-SCR) systems, Appl. Catal. B: Environ. 154–155 (2014) 339–349.
[31] J.H. Kwak, R. Tonkyn, D. Tran, D. Mei, S.J. Cho, L. Kovarik, J.H. Lee, C.H.F. Peden, J. Szanyi, Size-dependent catalytic performance of CuO on γ-Al_2O_3: NO reduction versus NH_3 oxidation, ACS Catal. 2 (2012) 1432–1440.
[32] M. Jabłońska, M. Nocuń, K. Gołąbek, R. Palkovits, Effect of preparation procedures on catalytic activity and selectivity of copper-based mixed oxides in selective catalytic oxidation of ammonia into nitrogen and water vapour, Appl. Surf. Sci. 423 (2017) 498–508.
[33] M. Amblard, R. Burch, B.W.L. Southward, A study of the mechanism of selective conversion of ammonia to nitrogen on Ni/γ-Al_2O_3 under strongly oxidising conditions, Catal. Today 59 (2000) 365–371.
[34] M.A. Larrubia, G. Ramis, G. Busca, An FT-IR study of the adsorption and oxidation of N-containing compounds over Fe_2O_3-TiO_2 SCR catalysts, Appl. Catal. B: Environ. 30 (2001) 101–110.
[35] G. Ramis, M.A. Larrubia, G. Busca, On the chemistry of ammonia over oxide catalysts: Fourier transform infrared study of ammonia, hydrazine and hydroxylamine adsorption over iron—titania catalyst, Top. Catal. 11 (2000) 161–166.
[36] W.S. Kijlstra, D.S. Brands, E.K. Poels, A. Bliek, Mechanism of the selective catalytic reduction of NO by NH_3over MnO_x/Al_2O_3, J. Catal. 171 (1997) 208–218.

[37] H. Zou, J. Shen, Microcalorimetric and infrared spectroscopic studies of γ-Al_2O_3 modified by zinc oxide, Thermochim. Acta 351 (2000) 165–170.
[38] J.G. Amores, V.S. Escribano, G. Ramis, G. Busca, An FT-IR study of ammonia adsorption and oxidation over anatase-supported metal oxides, Appl. Catal. B: Environ. 13 (1997) 45–58.
[39] G. Ramis, L. Yi, G. Busca, M. Turco, E. Kotur, R.J. Willey, Adsorption, activation, and oxidation of ammonia over SCR catalysts, J. Catal. 157 (1995) 523–535.
[40] K. Shimizu, J. Shibata, H. Yoshida, A. Satsuma, T. Hattori, Silver-alumina catalysts for selective reduction of NO by higher hydrocarbons: structure of active sites and reaction mechanism, Appl. Catal. B: Environ. 30 (2001) 151–162.
[41] C. Yu, L. Wang, B. Huang, In situ DRIFTS study of the low temperature selective catalytic reduction of NO with NH_3 over MnO_x supported on multi-walled carbon nanotubes catalysts, Aerosol Air Qual. Res. 15 (2015) 1017–1027.
[42] K.I. Hadjiivanov, Identification of neutral and charged N_xO_y surface species by IR spectroscopy, Catal. Rev. 42 (2000) 71–144.
[43] P. Sazama, L. Čapek, H. Drobná, Z. Sobalík, J. Dědeček, K. Arve, B. Wichterlová, Enhancement of decane-SCR-NO_xover Ag/alumina by hydrogen. Reaction kinetics and in situ FTIR and UV–vis study, J. Catal. 232 (2005) 302–317.
[44] L. Zhang, H. He, Mechanism of selective catalytic oxidation of ammonia to nitrogen over Ag/Al_2O_3, J. Catal. 268 (2009) 18–25.
[45] W. Chen, Y. Ma, Z. Qu, Q. Liu, W. Huang, X. Hu, N. Yan, Mechanism of the selective catalytic oxidation of slip ammonia over Ru-modified Ce-Zr complexes determined by in situ diffuse reflectance infrared Fourier transform spectroscopy, Environ. Sci. Technol. 48 (2014) 12199–12205.